A High Resolution Radio Survey of Class I Protostars

P.W.Lucas[1,2], Katherine M.Blundell[2] and P.F.Roche[2]

[1]Dept. of Physical Sciences, University of Hertfordshire, College Lane, Hatfield AL10 9AB.
email: pwl@star.herts.ac.uk

[2]Astrophysics Dept., University of Oxford, 1 Keble Road, Oxford OX1 3RH.

Accepted by MNRAS

Abstract

We report the results of a survey of low mass Class I protostars in the cm continuum. In the initial survey, seven sources in the Taurus star formation were observed with the VLA at 0".25 resolution. All seven sources drive CO outflows and display Herbig-Haro flows in the optical or near infrared wavebands. 4/7 sources were detected, two of which are new discoveries in systems of very low luminosity, one being the lowest luminosity system detected to date in the cm continuum. Notably, three sources were not detected to a 3-σ limit of 0.10 mJy/beam, which indicates that significant cm continuum emission is not a universal feature of Class I systems with outflow activity. Subsequent observations of HH30, a more evolved Class II system, found no emission to a 3-σ limit of 0.03 mJy/beam. After comparison with near infrared data, we suggest that the discriminating feature of the detected systems is a relatively high ionisation fraction in the stellar wind. Temporal variability of the outflow may also play a role: only recently ejected knots may have sufficiently dense plasma to be optically thick to free-free emission, and hence produce detectable flux. The one relatively bright source, IRAS 04016+2610 (L1489 IRS), is clearly resolved on a 0".4 scale at 2 cm and 3.5 cm. Follow-up imaging with MERLIN did not detect this source with a 0".04 beam, indicating that the radio emission is generated in a region with a radius of ≈ 25 au, which is broadly similar to the radius of the bipolar cavities inferred from models of near infrared data. Interpretation of this system is complicated by the existence of a quadrupolar outflow, i.e. two bipolar outflows along roughly perpendicular axes, which we originally detected through polarimetric imaging. We present a near infrared H_2 image in which a bow shock in the secondary outflow is clearly seen. This complicated structure may have been caused by a gravitational interaction between two protostars.

1 Introduction

For many years it has been known that some Young Stellar Objects (YSOs) are sources of radio emission in the cm continuum. The more deeply embedded YSOs, now commonly referred to as Class I and Class 0 protostars, exhibit the 'thermal' spectrum of free-free radio emission between 2 and 6 cm. At shorter wavelengths continuum emission from cold circumstellar dust becomes the dominant source of radiation (Rodriguez 1994). The energy source for the ionisation and free-free emission in low mass YSOs is still unknown. As the sensitivity of radio telescopes has improved, free-free emission has been detected from an increasing number of protostars, particularly those with CO outflows and associated Herbig-Haro flows. Rodriguez and Reipurth (1996) suggested that that all such systems may be radio sources.

We have conducted a sensitive survey of a small sample of Class I YSOs in the Taurus molecular cloud which exhibit outflow activity. The aim was to discover whether significant radio emission is indeed a universal feature of such systems and, by comparison with near infrared data, to shed light on the process which produces it. By observing at high spatial resolution we also hoped to probe the structure of the circumstellar matter on the scale of the solar system. The radio emission might trace the structure because shock-ionisation of the outflow where it is collimated by the molecular envelope is a long-standing hypothesis to explain the free-free emission. It transpired that most Class I sources are too faint for detailed mapping to be achieved with present radio receiver technology but some useful spatial information was obtained.

The initial survey and follow-up observations at radio and infrared wavelengths are described in Section 2. The results are detailed in Section 3 and in Section 4 we discuss the possible explanations for the differing radio fluxes of otherwise similar protostars. Our conclusions are presented in Section 5.

2 Observations

2.1 Radio Observations

We selected a sample of seven low mass YSOs from the nearby Taurus-Auriga star forming region which we have previously studied in the near infrared waveband. These systems all display Herbig-Haro jets or knots of ejected nebulosity at near infrared or optical wavelengths (Lucas & Roche 1997 (hereafter LR97); 1998 and references therein) and all possess CO outflows (Moriarty-Schieven et al. 1992). Bolometric source luminosities are given in Table 1. We will refer to these sources by their IRAS coordinate designations. One of the eight sources from the near infrared sample, 04187+1836 (L1551-IRS5), was not observed since it had already been the subject of several radio investigations (Bieging & Cohen 1985; Rodriguez et al. 1986).

The initial observations were conducted with the VLA in A configuration on 14 December 1996. Each source was observed in X band (3.5 cm), the most sensitive wavelength for these observations, with on-source integration times of 36 minutes. Three sources were also observed with varying integration times in U band (2 cm) in order to provide higher spatial resolution and information about the spectral energy distribution. Two of these three sources (IRAS 04016+2610 and IRAS 04361+2547) had previously been detected at cm wavelengths (Rodriguez et al. 1989; Terebey, Vogel & Myers 1992) but none of the others had previously been studied in this waveband. The observations of each source were separated in time in order to provide good *uv* plane coverage. The flux calibrator was 3C48 and the phase calibrator was 0400+258, the latter being observed every 10-15 minutes to permit accurate phase calibration. Atmospheric conditions were stable, permitting the collection of high quality data in both X band and U band. In A configuration the spatial resolution is ≈ 0.22 arcsec (FWHM) at 3.5 cm and ≈ 0.13 arcsec at 2 cm. At the distance of the Taurus molecular cloud, 140 pc, 0.22 arcsec corresponds to 30 au.

Roughly simultaneous observations were conducted with MERLIN between 20 November and 17 December 1996 and follow-up observations were made later with the VLA. 04016+2610 (L1489 IRS) and 04302+2247 were observed with MERLIN and so was HL Tau, a previously known radio source, at the request of the MERLIN Panel for the Allocation of Telescope Time. These observations were made between 20 November and 17 December 1996, with integration times of between 10 and 16 hours in each case. Six elements of MERLIN were used, observing at C band (6 cm). The flux calibrator was 3C48 and the phase calibrator was 0400+258. At this frequency MERLIN has a beam size of 0.04 arcsec (6 au at 140 pc), so it is most sensitive to very compact emission on sub-solar system scales for these objects.

Deeper follow-up mapping with the VLA was conducted on 29 May 1998, again in A configuration. 04016+2610 was observed in U band, in or-

der to maximise spatial resolution at the expense of sensitivity, with an on-source integration time of 4 hours and 49 minutes. 04302+2247 and 04239+2436 were observed at X band, each with an integration time of 1 hour and 48 minutes. The flux calibrator was 3C286 and the phase calibrator was 0400+258. Observations of HH30, a system famous for its directly observed accretion disk and prominent bipolar jet, were made with the VLA in D configuration on 17th March 1999. The integration time was 4 hours, observing at X band for best sensitivity. The flux calibrator was 3C48 and the phase calibrator was 0400+258. All the datasets were reduced and analysed with the AIPS software package, using standard techniques.

2.2 Near Infrared Observations

Near infrared observations were made with the 3.8-m United Kingdom Infrared Telescope (UKIRT). 04016+2610 was observed with UFTI, the UKIRT Fast Track Imager, on 5 October 1998 during its commissioning period at UKIRT. UFTI is a common-user near infrared camera with a 1024^2 HgCdTe HAWAII array, designed for high resolution imaging with the recently upgraded UKIRT in the 0.8-2.5 μm region. UFTI was constructed at Oxford University by a team led by the authors. Descriptions of the instrument design and of operational details are available on the world wide web (Roche & Lucas 1998 and Leggett 1998). 04016+2610 was imaged in the (1-0) S(1) line of H_2 at 2.12 μm and in K band, in order to probe the unusual outflow structure of the system. The new K filter optimised for Mauna Kea, which will be employed by the Gemini telescopes, was used. It is very similar to the standard Barr K filter (2.00-2.40 μm). The integration times were 900 s and 580 s in the H_2 and K filters respectively. Thin and variable cloud was present but the throughput was not seriously diminished. Seeing conditions were fairly good, with a FWHM of 0.7 arcsec seen for field stars even though the tip/tilt function of the UKIRT secondary mirror could not be used inside the L1489 dark cloud, due to lack of optically bright guide stars. The image scale is 0.091 arcsec/pixel. Median filtered flatfields were constructed from nine point image mosaics. The core of the source was close to saturation in the K band data, leading to a loss of photometric accuracy at the flux peak. In this paper we examine the extended outflow structure so this is of little concern. The observers were PFR, PWL and Sandy Leggett.

04016+2610 was also observed in the L′ band (3.5-4.1 μm) with IRCAM-3, the other near infrared camera at UKIRT, which has a 256^2 InSb array, which is sensitive up to 5.5μm in the thermal infrared. The integration time was 240 s and the plate scale was 0.284 arcsec/pixel. These observations were made by Sandy Leggett on 30 September 1998 as part of the UKIRT Service programme.

A 2 μm spectrum of 04302+2247 was obtained with CGS4, the near infrared spectrograph at UKIRT, on 30 November 1999. This system has not been included in previous spectroscopic surveys of YSOs, so the spectrum was obtained to investigate outflow activity via the H_2 and Brackett γ emission lines at 2.12 and 2.17 μm respectively. CGS4 has an InSb array of the same type as IRCAM-3. The 40 l/mm grating was used, giving a dispersion of 2.5 nm per pixel and spectral coverage from 1.9 to 2.5 μm. The slit width was 2 pixels, corresponding to 1.2 arcsec on the sky, and the slit position angle was 87.1 degrees, roughly parallel to the axis of the circumstellar envelope. The effective spectral resolution was 440 and the array was stepped twice at each sky position in a 1 pixel step to remove bad pixels. The integration time was 672 s. All of the infrared datasets were reduced with the IRAF software package.

3 Results

3.1 The Initial Survey

3.1.1 VLA Data - 1st Epoch

Of the seven sources observed one, 04016+2610 (L1489 IRS), was clearly detected at 3.5 cm and 2 cm. However the 2 cm emission is visible only when the data are tapered to the resolution of the 3.5 cm data, $\approx$ 0.22 arcsec, indicating that this source may be resolved out on smaller scales. Three other sources were weakly detected at 3.5 cm at the 4.5-5.0-σ level: 04361+2547 (TMR-1), 04302+2247 and 04239+2436. At 2 cm, 04361+2547 and 04302+2247 were observed and point sources were marginally detected at the same positions with even lower signal to noise (see Table 1). The three weak detections are consistent with emission from point sources but extended emission cannot be ruled out with confidence. The other 3 sources possess no radio counterparts to a 3-σ limit of $\approx$ 0.10 mJy/beam. The noise in interferometer data is non-Gaussian and can behave unpredictably. Consequently, it is common to require 5-σ for a secure detection but a 3-σ limit can be taken as a reliable non-detection when the position is known. In the case of 04302+2247, a combination of Digi-

tal Sky Survey and archival Hubble Space Telescope data allowed us to determine that the radio candidate lay within 1 arcsec of the faint optical counterpart, indicating an almost certain correspondence. For 04239+2436, the published infrared positions were only accurate to 3 arcseconds so confirmation had to await the second, deeper set of VLA data.

The maps of 04016+2610 are displayed in Figure 1(a-b), and a near infrared comparison image in polarized intensity (surface brightness multiplied by degree of polarization) is reproduced from LR97 in Figure 2. At 3.5 cm we see a point source with extension to the northwest and at 2 cm the structure is similar but the extended emission is only marginally detected in approximately the same direction. The spatial scale of the extension is ≈ 0.4 arcsec (50 au) and we see that it is not aligned with the outflow cavities visible in the infrared image. In LR97 we interpreted the near infrared structure as a 'quadrupolar outflow', i.e. two perpendicular bipolar flows, perhaps indicative of an unresolved binary system. The approximate directions of the primary and secondary outflows (so named for their relative prominence) are marked in Figure 2.

Two point spectral indices can be very roughly estimated for the 3 sources for which we have both X and U band data, using the data in Table 1. In each case the data imply a small positive index: $0 < \alpha < 2$ where the flux density S_ν at frequency ν is described by $S_\nu \propto \nu^\alpha$. This is consistent with free-free emission from partially ionised gas, rather than the continuum emission from cold dust. Gyro-synchrotron emission cannot be ruled out entirely but no circular polarization is detected in 04016+2610 above a 3-σ limit of 32% at 3.5 cm.

3.1.2 MERLIN Data

None of the three sources which were observed with the 0.04 arcsec MERLIN beam were detected at 6 cm (see Table 1). 04016+2610 has a flux of 0.5 mJy at 6 cm, measured by Rodriguez et al.(1989) at low spatial resolution, but it was not detected to a 3-σ limit of 0.26 mJy/beam. The non-detection of 04016+2610 is therefore significant and demonstrates that the radio emission arises on spatial scales of tens of astronomical units, comparable to the size of the solar system. This is consistent with the VLA 2 cm data, which also appear to be on the verge of resolving out the emission, as described above. Since the VLA and MERLIN observations were obtained within a few days of each other it is unlikely that source variability could account for the MERLIN non-detection. HL Tau has a 6 cm flux of only ≈ 0.22 mJy (Wilner et al. 1996) so the MERLIN data do not provide useful information on this object. Similarly, the faintness of the 3.6 cm emission from 04302+2247 is consistent with the non-detection by MERLIN, assuming a thermal spectrum.

3.2 Further Observations

3.2.1 VLA Data

The 1998 observations of 04302+2247 and 04239+2436 confirm the detections of these sources (see Table 1) at the same location as the 1st epoch candidates. The fluxes measured at the 2 epochs are the same within the 1-σ errors and both systems appear to be unresolved on a scale of 30 au. 04302+2247 is the lowest luminosity YSO from which radio emission has so far been detected, with $L_{bol} \approx 0.3\ L_\odot$, and 04239+2436 is only slightly more luminous with $L_{bol} \approx 1.2\ L_\odot$ (Tamura et al. 1991). The low luminosities make it most unlikely that photoionisation is responsible for ionising the outflow, (see Section 4.2.2).

In the 1998 data the morphology of 04016+2610 appears to have changed: only a point source is detected, with no sign of the extended emission desite the greater sensitivity of the observations. The source remains visible at the full resolution of the VLA at 2 cm, which is $0^{\text{"}}.136 \times 0^{\text{"}}.113$ in a "robust zero" map (which adds some weight to the longer baselines with only a minimal reduction in signal to noise, relative to a naturally weighted map). The image profile is not perfectly symmetric but the JMFIT beam-fitting task in AIPS indicates that the data are consistent with a point source. It is probable that this is a real change in source morphology, related to the outflow activity of the protostar but the peak flux density does not appear to have changed between the two epochs.

The deep integration at the location of HH30 in 1999 failed to detect this system to a 3-σ limit of 0.03 mJy at 3.5 cm. This system was also undetected to a limit of ≈ 0.1 mJy in 3.5 cm observations of the HL Tau/HH30 region made in 1992 by Luis Rodriguez (private communication).

3.3 Infrared Data

3.3.1 04016+2610

The K band and H_2 images of 04016+2610 are displayed in Figure 3(a,b). The most striking feature in H_2 is a well defined, V-shaped, emission nebulosity to the south of the core, which we interpret as a bow-shock in the secondary outflow of the system.

In the continuum image this bow shock is mostly obscured by the surrounding reflection nebulosity. The nebulosity also extends several hundred au to the north and a resolved continuum source (IRS2) is visible close to the core in this direction, coincident with the feature seen in polarized intensity in Figure 2. These features support the inference of a secondary bipolar outflow along the direction indicated in Figure 2. It is oriented roughly perpendicular to the primary east-west outflow but is not clearly visible in existing high resolution imaging (non-polarimetric) data (LR97 and Padgett et al. 1999). Although IRS2 appears rounded in our relatively low resolution data, the high resolution 3-colour NICMOS data of Padgett et al. reveal that IRS2 has a triangular shape which is consistent with a conical cavity in the nebula that is illuminated by a source at or close to the central flux peak. The quadrupolar outflow structure is also indicated in the CS (J=2-1) map of Ohashi et al.(1996), although the velocity distribution of the low density gas depicted there is more consistent with *infalling* material.

The H_2 and K images were normalised such that the same flux was received in both filters from a nearby field star in the images before subtracting to produce the image in Figure 3(c). Since the field star lies within or behind the L1489 dark cloud, the effect of the extinction by the cloud is cancelled to some degree. Hence, the solid (positive) contours represent nebulosity which appears bluer than the field star in the (H_2-K) colour, due either to H_2 emission or a bluer K band continuum, while the dotted (negative) contours represent redder radiation. The bow shock is the only feature in Fig. 3(c) which we attribute to H_2 emission. The rest of the structure in Fig.3(c) is real, except at the flux peak (marked with an asterisk), which appears positive owing to saturation at K band. The blue colour of the southeastern nebulosity is consistent with Rayleigh-like scattering in the K band ($F_\lambda \propto \lambda^{-4}$), which was indicated by the very high ($> 70\%$) degrees of linear polarisation measured in this system (LR97). The red nebulosity near the flux peak corresponds to the densest material where the scattered light is strongly reddened by extinction. Our interpretation of the residuals as variations in colour across the K band (2.0-2.4 μm) is consistent with the Padgett et al. data, which also shows that the reddest nebulosity lies to the northwest, while the southeastern material is bluer. If the system is a binary then it could either be unresolved by NICMOS (separation $\lesssim 0\overset{\text{“}}{.}1 = 14$ au, depending on the relative brightness) or an unseen component may lie obscured behind the very red, dense material to the northwest of the central flux peak. This latter possibility is suggested by the shape of the putative conical cavity, IRS2, which appears to focus on a point at least 1 arcsec northwest of the primary flux peak.

The L′ data in Figure 4 show a cometary nebula similar in appearance to the K band continuum data, with no sign of the secondary outflow. It appears that sub-arcsecond millimetre continuum data will be needed to discover the distribution of matter in this unusual system.

3.3.2 04302+2247

The 2 micron spectrum of 04302+2247 (Figure 5) rises toward longer wavelengths and shows emission lines of Brγ, Brδ and the H_2 (1-0)S(1) transition. None of the other H_2 lines are clearly detected. The equivalent widths are $EW_\lambda(Br\gamma) = 14.5 \pm 2.1$Å and $EW_\lambda(H_2) = 5.2 \pm 1.0$Å respectively. Br$\delta$ is blended with a telluric absorption feature and is hard to measure. The Brγ equivalent width is exceptionally large for a Class I protostar, but the H_2 line strength line is only slightly above average (see Greene & Lada 1996a). The Brγ equivalent width is similar to that of 04239+2436 (Greene & Lada 1996b) which is notable for its extreme near infrared spectrum. However, 04302+2247 differs from 04239+2436 in that it does not show the CO (v=2-0) transitions in emission, only marginally detected features in absorption. The core of the system is obscured at near infrared wavelengths and the Brγ emission is thought to originate in the hot, dense conditions close to the star, so we presume that this line is observed in scattered light. The strong Brγ but weaker H_2 implies that the wind of 04302+2247 has an unusually high temperature or ionisation fraction.

3.3.3 04239+2436

In an earlier paper (Lucas & Roche 1998) we presented broad band imaging polarimetry of this system and noted that a possible jet-like feature was marginally detected along the symmetry axis of the circumstellar envelope but was mostly obscured by the nebulosity. High resolution near infrared images of this system were obtained with NICMOS on the Hubble Space Telescope (HST) in 1998 (PI Reipurth, data in preparation). The 1.6μm broad band image in the HST archive (not shown) clearly resolves a well collimated knotted jet along the symmetry axis. This prominent outflow is clearly related to the extreme outflow activity implied by the

near infrared spectrum of Greene & Lada. The detection of radio emission in two systems with exceptionally strong HI emission lines, 04239+2436 and 04302+2247, is interesting. However, the radio sources 04016+2610 and 04361+2547 have unremarkable HI emission.

4 Discussion and Interpretation

4.1 04016+2610 and Cavity Radii

The observation that radio emission in 04016+2610 arises on a scale of 50 au, or 25 au radius, is important because it sets a lower limit on the cavity radius in the core, where the two bipolar cavities presumably merge into a single cleared space. This important parameter was inferred from near infrared Monte Carlo modelling of YSOs as being about 25 au (eg. LR97) but has never been well constrained. Admittedly 04016+2610 is far from an ideal test case, being a very complicated system and probably a binary, but this is also the spatial scale of the gyrosynchrotron emission observed around T Tau South by Ray et al.(1997) using MERLIN. Hence we can have a little more confidence in inferences drawn from near infrared simulations.

We speculate that the origin of the strange quadrupolar outflow geometry in 04016+2610 lies in a gravitational interaction between stars which formed in separate protostellar cores and later underwent a close encounter. Hydrodynamical simulations of such scenarios have been performed by Boffin et al.(1998) for star-disc encounters and Watkins et al.(1998a, 1998b) for disc-disc encounters. These simulations show that a number of bodies may be produced in such encounters, and their rotation axes need not be parallel.

4.2 The Criterion for Detectable Radio Emission

The reason why some YSOs emit detectable centimetre continuum flux and others do not has been puzzle since the 1980s. Gibb (1999) recently reviewed the problem using a large dataset and showed that radio emission is relatively common among young (Class I and Class 0) sources and among chromospherically active Class III sources, which are presumed to emit gyrosynchrotron radiation, but rare in Class II systems. We are concerned here with the younger group of radio emitters, all of which drive molecular outflows. Rodriguez (1994) stated that 40/180 of the then known molecular outflow sources were radio emitters, and suggested that this 22% fraction may increase as more sensitive surveys are carried out. Gibb suggested that the polar orientation of the system might be an important factor, owing to self-absorption in optically thick systems viewed close to the outflow axis. This probably does have some effect but since the great majority of YSOs are not viewed close to pole-on there must be an additional explanation for the non-detection of a large fraction of Class I sources.

4.2.1 Variability

Reviewing the results of our initial radio survey and the confirmatory detections of 04302+2247 and 04239+2436 in the 2nd epoch, we note that the outflows of the 4/7 detected sources all display good evidence for an ongoing or recent ejection event. In the infrared, 04016+2610 has a marginally resolved secondary continuum source close to the core - probably a knot of gas and dust in the secondary outflow. 04239+2436 has extremely active near infrared line emission and a powerful Herbig-Haro jet. 04302+2247 has a quadrupolar structure in the infrared, which has been attributed to outflowing material within 200 au of the core, either along the outflow axis (Lucas & Roche 1997) or flowing along the cavity walls (Padgett et al. 1999). Finally, 04361+2547 (TMR-1) is a resolved binary with an asymmetric core structure and a possible low mass companion which appears to be connected to the system by a long channel of reflected light (Terebey et al. 1998,2000). In this case outflow actvity is hard to separate from the confused nebular strcture. Admittedly, the undetected radio sources also display infrared outflow activity but in the form of quite discrete Herbig-Haro knots rather than a jet. Hence it is possible that the source of the outflow was quiescent at the time of observation.

The apparent radio variability of 04016+2610 suggested the following scenario: a Class I protostar ejects a roughly spherical knot of partially ionised gas at intervals of a few years, which expands and becomes more rarefied until it is optically thin to free-free emission. As shown by Martin (1996) the radio flux from such an isothermal stellar wind or knot is given by:

(1) $S_\nu(T) = \frac{2k_B T\nu^2}{c^2 d^2} \int_A (1 - e^{-\tau(\nu,T)}) dA'$

(2) $\tau = \int \kappa(\nu, T) n_e^2 ds$

assuming that the Planck function is appropriate in the optically thick limit. Hence, the flux from an expanding knot will rapidly decline when the the optically thin threshold is passed. Unfortunately, the electron number density, n_e, is very

poorly constrained for knots near the point of origin: for continuous wind models Martin found that models with an electron density at 1 au from the star in the range 10^7 to 10^{12} cm^{-3} can match observed fluxes and spectral indices. Moreover, radio variability data on timescales of a few years is very sparse.

To test this idea we undertook the observation of the Class II system HH30. It has a very prominent, well collimated jet with knots observed within a few dozen au of the star (Burrows et al. 1996), apparently ejected at intervals of order 1 year and the jet can be observed to within 30 au of the source, making it ideal for comparative radio/optical studies. (We assume here that the knots are discrete ejections rather than shocks in a steady flow). However, no radio source was detected to the stringent limit of 0.03 mJy/beam at 3.5 cm in 1999, nor in 1992 above 0.1 mJy/beam. A similar but younger system (Class I or Class 0) is HH212 (Zinnecker, McCaughrean & Rayner 1998). HH212 also has a well collimated and knotted jet in which the perfect bipolar symmetry of the knots indicates that they do represent discrete ejections of matter. HH212 might be expected to have a higher rate of outflow and a stronger radio flux given its evolutionary status. However, Zinnecker et al. also detected no radio source to a 4-σ limit of 0.06 mJy/beam. These non-detections could simply be due to observation in a quiescent period of outflow activity, especially in the case of HH212, where the knots are ejected at 5 year intervals. However, we must conclude that the radio variability hypothesis is given no support by these limited data, and large amplitude radio variability has not, to our knowledge, yet been observed in these systems.

4.2.2 Ionisation

Another possibility suggested by eq.2 is that the number density of electrons is low in radio quiet systems due to a low ionisation fraction. Reynolds (1986) calculated that $S_\nu \propto n_e^{1.67}$ for an isothermal collimated wind. This is a slightly weaker dependence than the n_e^2 relation for an optically thin wind but an order of magnitude reduction in radio flux would be caused by less than a factor of 4 difference in the ionisation fraction. The other important variable, temperature, has a relatively weak effect on the source function. As mentioned in Section 1, the origin of the ionisation is unknown. Photoionisation by the photospheric UV radiation is insignificant for cool low mass YSOs. Boundary layer emission where matter accretes on to the stellar surface does not seem likely, given that modelling of the UV continuum in classical T Tauri stars by Gullbring et al.(1998) indicates temperatures of only about 10000 K. Shock ionisation of the wind remains a serious possibility. Delamarter, Frank & Hartmann (2000) have conducted numerical simulations of the interaction of a spherical wind and an equatorially condensed circumstellar envelope. Their results show that physical collimation of such a wind by the envelope does produce cavity structures consistent with near infrared and millimetre imaging data. Bacciotti & Eisloffel (1999) have directly and precisely measured the ionisation of the knots in several stellar jets, under the assumption that the ionisation states of nitrogen and oxygen are maintained by charge transfer with hydrogen. They have shown that the ionisation fraction, $x_e = n_e/n_H$, typically lies in the range $x_e = 5$ to 35% but can be as low as 1.5% (in parts of the HH34 jet). Denser and less excited jets tend toward the smaller values. In general, for a given section of the jet the ionisation fraction appears to decline slowly with increasing distance from the source but the fraction in separate sections is uncorrelated. Thus, a newly ejected knot can have a low level of ionisation, as in the case of HH24E for example. Clearly, a negligible ionisation fraction is not consistent with the prominent Hα and [SII] emission which has been observed with HST.

The best available spectroscopic data on the HH30 jet is given by Mundt et al.(1990), which is relatively low resolution ground-based data, but includes the necessary [OI], [NII], [SII] and Hα lines. We attempted to apply the Bacciotti method to the printed data and a low ionisation fraction appeared plausible, but the problem has very recently been fully addressed by the pioneers of this technique, see Bacciotti, Eisloffel & Ray (1999). They combined the Mundt et al. spectra with HST emission line images from 1995 to probe conditions with very fine resolution, with the caveat that possible temporal changes in electron density and excitation may cause errors. They find $x_e = 6.5\%$ at the base of the jet and that x_e actually rises slowly to 14% at 300 au from the source. The low ionisation fraction at source supports our hypothesis that this may be the reason why the system is radio quiet. We must caution that they have measured x_e in relatively low density conditions ($n_e < 10^4$ cm^{-3}), compared to those which must prevail on small spatial scales at the source of the jet. The hydrogen gas density in the jet measured by Bacciotti et al. is unusually high compared to other systems, which indicates that the very low radio flux cannot be attributed simply to insufficient material. In their

analysis they also argue that the observed bright knots are not regions of high density but merely to local shocks. This is a controversial point but if true it would mean that gas density is sufficient for radio emission at all times.

Is the ionisation fraction therefore the discriminating factor for radio emission from Class I sources? If we take $x_e = 15\%$ as the average value and 6.5% in HH30 then the system might be a factor of 5 fainter than average, assuming $S_\nu \propto x_e^2$. The actual dependence of flux density on x_e is a function of the wind geometry in the core, as described by Reynolds (1986), and may well be weaker. 3/4 of the radio protostars detected in our Taurus sample have fluxes of only 0.10-0.15 mJy, so low ionisation may be just sufficient to account for a flux density below our upper limit of 0.03 mJy/beam, particularly if the ionisation fraction is even lower than normal in the dense radio emitting region. If so, then why is the ionisation fraction low in HH30 ? Both HH30 and HH212 have very well collimated jets and the observed disk of HH30 is confined to equatorial latitudes. Thus the jet might avoid shock-ionisation by interaction with the surrounding envelope while poorly collimated outflows such as that of 04302+2247 do not. It is hard to assess the collimation of most of the outflows in our sample since in most cases the infrared nebulosity prevents clear delineation of the outflow. 04239+2436 has a well collimated jet in the NICMOS data and is a radio source but poorly collimated optical [SII] emission was observed by Gomez et al.(1997) to one side of the system's axis of symmetry. Some well collimated jets (eg. HH34) are radio bright but their envelope structure is largely obscured from view. Direct imaging of jet/envelope interactions will have to be undertaken using adaptive optics on 8-m class telescopes.

5 Conclusions

Observation of a small sample of low mass Class I protostars indicates that radio emission at above the level of 0.1 mJy/beam is far from ubiquitous. We suggest that the radio quietness in sources with active Herbig-Haro flows might be accounted for by a relatively low ionisation fraction, at the level of a few percent. The ionisation fraction could plausibly be related to the collimation of the outflow, particularly if shock-ionisation by interaction with the circumstellar envelope plays a role. In addition, radio variability due to unsteady outflows may also occur and this should be investigated by monitoring known radio emitters.

In 04016+2610 (L1489 IRS) a well defined bow shock is observed in 2.12 μm H_2 radiation along the line of the secondary bipolar cavity revealed in a polarised intensity image. This provides further evidence for a quadrupolar flow. We suggest that the system is the product of a gravitational interaction between two young solar systems, which produced a binary star whose components drive outflows along different axes of rotation. The system may be an unresolved binary (separation $\lesssim 0\text{“}.1$ or 14 au), or the secondary component may be obscured by dense material in the core of the system.

6 Acknowledgements

We are grateful to the VLA Time Allocation Committee for awarding us substantial amounts of time for this project. We especially wish to thank Mike Rupen of the VLA Array Operations Centre, Socorro for his help in calibrating and reducing the data, and also his colleagues for their hospitality. We also thank the MERLIN Time Allocation Committee giving us time to set some upper limits and Simon Garrington for his help in reducing the data. We also wish to thank everyone at Oxford, Edinburgh Cambridge and the Joint Astronomy Centre who participated in the design, construction and commissioning of UFTI at UKIRT. Special thanks go to Tony Handford, Keith Nobbs and Phil Evans of the Nuclear and Astrophysics Department workshop in Oxford, for transforming the designs into real metal. UKIRT and the Joint Astronomy Centre are operated on behalf of the UK Particle Physics and Astronomy Research Council.

References

Bacciotti F., & Eisloffel J. 1999, A&A 342,717
Bacciotti F., Eisloffel J., & Ray T.P. 1999, A&A 350,917
Bieging J.H., & Cohen M. 1985, ApJ 289, L5
Boffin H.M.J., Watkins S.J., Bhattal A.S., Francis N., & Whitworth A.P. 1998, MNRAS 300,1189
Burrows C.J., Stapelfeldt K.R., Watson A.M., Krist J.E., Ballester G.E., Clarke J.T., Crisp D., Gallagher J.S. III, Griffiths R.E., Hester J.J., Hoessel J.G., Holtzmann J.A., Mould J.R., Scowen P.A., Trauger J.T., Westphal J.A., 1996, ApJ, 473,437
Delamarter G., Frank A., & Hartmann L. 2000, ApJ 530,923
Gibb A. 1999, MNRAS 304,1
Gomez M., Whitney B.A., & Kenyon S.J. 1997, AJ 114,1138

Greene T.P., & Lada C.J. 1996a, AJ 112,2184
Greene T.P., & Lada C.J. 1996b, ApJ 461,345
Gullbring E., Hartmann L., Briceno C., & Calvet N. 1998, ApJ 492,323
Leggett S. 1998, www.jach.hawaii.edu/ukirt.new/instruments/ufti/ufti.html
Lucas P.W., & Roche 1997, MNRAS 286,895
Lucas P.W., & Roche 1998, MNRAS 299,699
Martin 1996, ApJ 473,1051
Moriarty-Schieven G.H., Wannier P.G., Tamura M., & Keene J. 1992, ApJ 400,260
Mundt R., Buehrke T., Solf J., Ray T., & Raga A.C. 1990, A&A 232,37
Ohashi N., Hayashi M., Kawabe R., & Ishiguro M. 1996, ApJ 466,317
Padgett D.L., Brandner W., Stapelfeldt K.R., Strom S.E., Terebey S., & Koerner D. 1999, AJ 117,1490
Ray T.P., Muxlow T.W.B., Axon D.J., Brown A., Corcoran D., Dyson J., & Mundt R. 1997. Nature 385,30
Reynolds S.P. 1986, ApJ 304,713
Roche P.F., & Lucas P.W. 1998, www-astro.physics.ox.ac.uk/ pwl/camera.html
Rodriguez, L.F., Canto J., Torrelles J.M., & Ho P.T.P. 1986, ApJ 301,L25
Rodriguez, L.F.; Myers, P.C.; Cruz-Gonzalez, I.; Terebey, S. 1989. ApJ 347,461
Rodriguez L.F. 1994, RMxAA 29,69
Rodriguez L.F., & Reipurth B. 1996, RMxAA 32,27
Tamura M., Gatley I., Waller W., & Werner M.W. 1991, ApJ 374,L25
Terebey S,, Vogel S.N., & Myers P.C. 1992. ApJ 390,181
Terebey S., van Buren D., Padgett D.L., Hancock T., & Brundage M. 1998. ApJ 507, L71
Terebey S., van Buren D., Matthews K., Padgett D.L. 2000. AJ 119.2341
Watkins S.J., Bhattal A.S., Boffin H.M.J., Francis N., & Whitworth A.P. 1998, MNRAS 300,1205
Watkins S.J., Bhattal A.S., Boffin H.M.J., Francis N., & Whitworth A.P. 1998, MNRAS 300,1214
Wilner D.J., Ho P.T.P.,, & Rodriguez L.F. 1996, ApJ 470,L117
Zinnecker H., McCaughrean M.J., & Rayner J.T. 1998, Nature 394,862

Table 1: **Results of the Survey**

Source	R.A. (1950)[a]	Dec (1950)	L_{bol}^{b}	3.5 cm Flux[c,d] (mJy)	2 cm Flux[c] (mJy)	6cm Flux[d] (mJy)
04016+2610 (L1489)	04 01 40.55	+26 10 47.7	3.7	0.343 ± 0.033	0.55 ± 0.11,0.52 ± 0.04	< 0.26
04361+2547 (TMR-1)	04 36 09.87	+25 47 28.7	2.8	0.14 ± 0.032	~ 0.30 ?	-
04302+2247	04 30 16.66	+22 47 04.4	0.33	0.16 ± 0.033,0.13 ± 0.02	~ 0.33 ?	< 0.32
04239+2436	04 23 54.42	+24 36 53.3	1.2	0.14 ± 0.033,0.10 ± 0.02	-	-
04325+2402	-	-	0.70	< 0.10	-	-
04248+2612	-	-	0.35	< 0.10	-	-
04365+2535	-	-	2.2	< 0.10	-	-
HH30	-	-	?	< 0.033	-	-
HL Tau	-	-	-	-	-	< 0.32

Notes:

a: Coordinates given are the locations of the radio sources.

b: Bolometric luminosities are from Tamura et al.(1991)

c: For 04016+2610 the fluxes given are flux densities/beam for the unresolved component. The extended flux is not well measured. Where two fluxes are given these are the first and second epoch measurements respectively.

d: upper limits are 3-σ, in mJy/beam.

Figure 1: Radio images of 04016+2610 (L1489) obtained with the VLA. (a) at 3.5 cm, (b) at 2 cm. The image in (b) has been tapered to the same resolution as (a) since the source vanishes in an untapered image. Beam sizes are marked. Contour levels in (a) are -0.079, -0.056, 0.056, 0.079, 0.112, 0.158, 0.224, 0.317 mJy and the 1-σ noise level is 0.033 mJy. Contour levels in (b) are -0.33, -0.22, 0.22, 0.275, 0.33, 0.385, 0.44, 0.495, 0.55 mJy and the 1-σ noise level is 0.11 mJy.

Figure 2: Near infrared image of 04016+2610 in polarised flux at 2.2 μm; reproduced from LR97. The central source is at the location of the flux peak in Figure 3(a), and is thought to be the protostar (or protostars if the system is an unresolved binary). Dense regions are suppressed because multiple scattering reduces the degree of polarisation. The dashed lines mark the approximate directions of the primary and secondary bipolar cavities as indicated by the contours. Contour levels are 0.0049, 0.0081, 0.013, 0.019, 0.032, 0.049, 0.065, 0.097, 0.13, 0.16, 0.20, 0.24, 0.32, 0.41, 0.49, 0.65, 0.81, normalised to unity at the peak.

Figure 3: Near infrared images of 04016+2510. (a) K band. (b) H_2 emission at 2.12 μm. (c) magnified view of the difference, H_2 - K, which has been smoothed slightly with a Gaussian ($\sigma = 1$ pixel). Contours are spaced at intervals of $\sqrt{2}$, normalised to the peak. A bow shock is visible in the direction of the secondary outflow in (b) but is mostly obscured by the reflection nebula in (a). The peak in (a) is saturated and a diffraction spike produces a horizontal ridge on the contours on either side. The structure in (c) is real, except at the location of the saturated flux peak (marked by an asterisk). The solid (positive) contours to the southeast of the peak represent regions where the scattered light at K band is very blue (effective wavelength $\lambda < 2.12$ μm), while the dotted (negative) contours are regions of high density where the scattered light has been reddened by extinction.

Figure 4: Near infrared image of 04026+2610 at L$'$ (3.8 μm). Each contour represents a step in surface brightness of a factor of 2. At this wavelength, the nebula depicts scattered light from dense material in the core of the system.

Figure 5: Near infrared spectrum of 04302+2247. The red continuum is typical of an embedded system. Brγ and Brδ are very prominent, but H_2 is relatively weak.

Figure 1

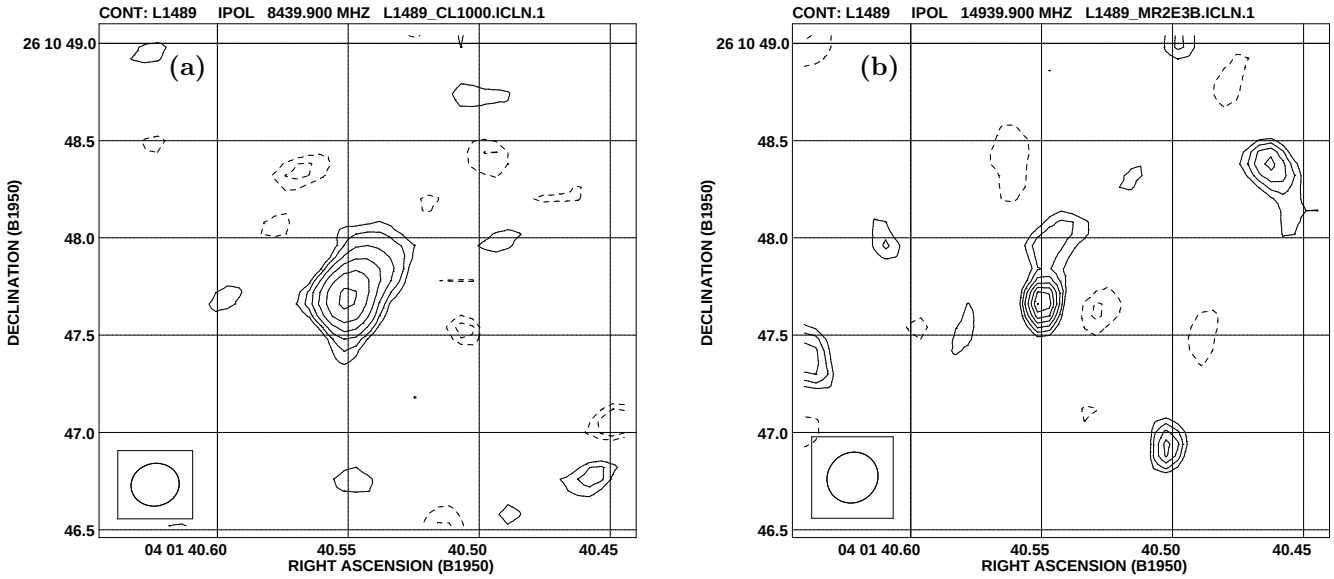
CONT: L1489 IPOL 8439.900 MHZ L1489_CL1000.ICLN.1
(a)
26 10 49.0
48.5
48.0
47.5
47.0
46.5
DECLINATION (B1950)
04 01 40.60
40.55
40.50
40.45
RIGHT ASCENSION (B1950)
CONT: L1489 IPOL 14939.900 MHZ L1489_MR2E3B.ICLN.1
(b)
26 10 49.0
48.5
48.0
47.5
47.0
46.5
DECLINATION (B1950)
04 01 40.60
40.55
40.50
40.45
RIGHT ASCENSION (B1950)

Figure 2

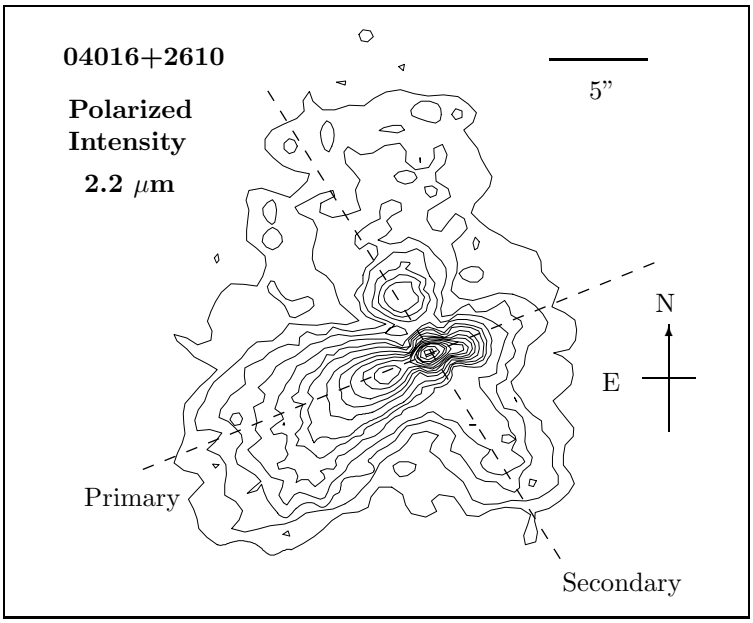
04016+2610
Polarized
Intensity
2.2 μm
5”
N
E
Primary
Secondary

Figure 3

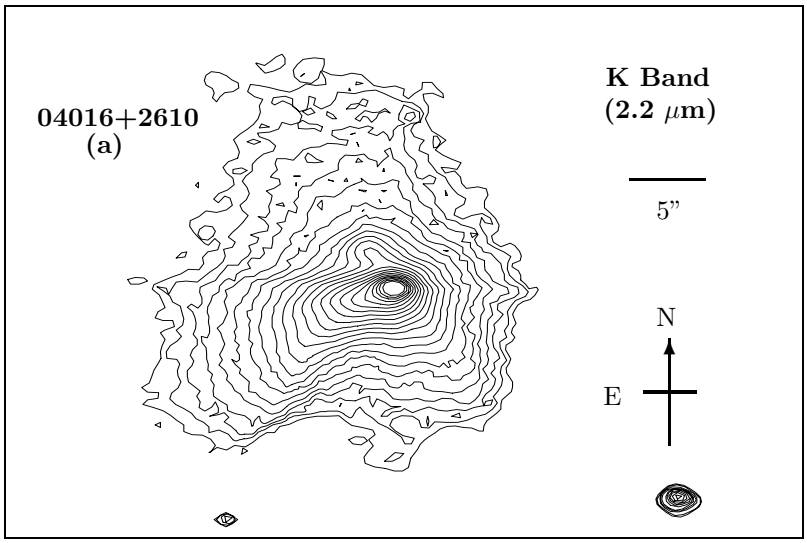
04016+2610
(a)
K Band
(2.2 μm)
5”
N
E

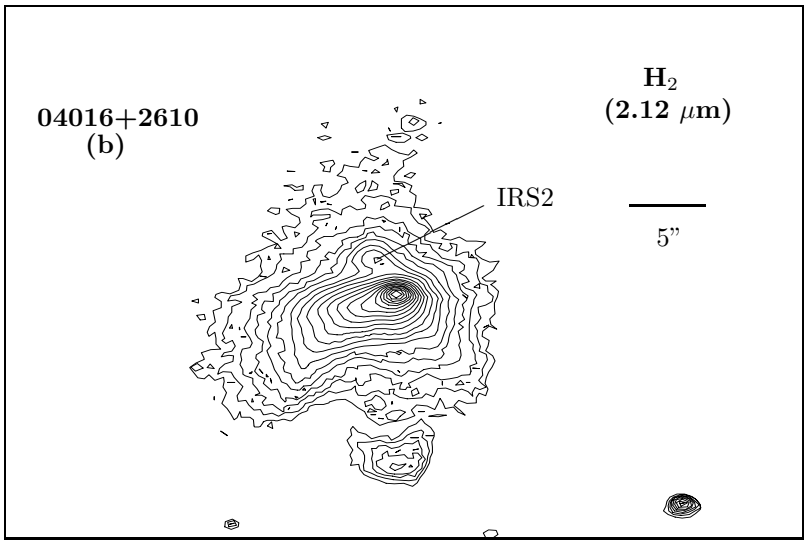
04016+2610
(b)
H2
(2.12 μm)
IRS2
5”

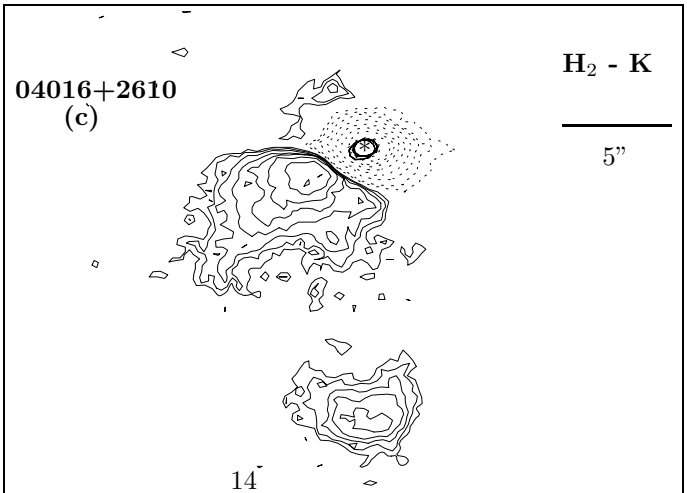
04016+2610
(c)
H2 - K
5”

Figure 4

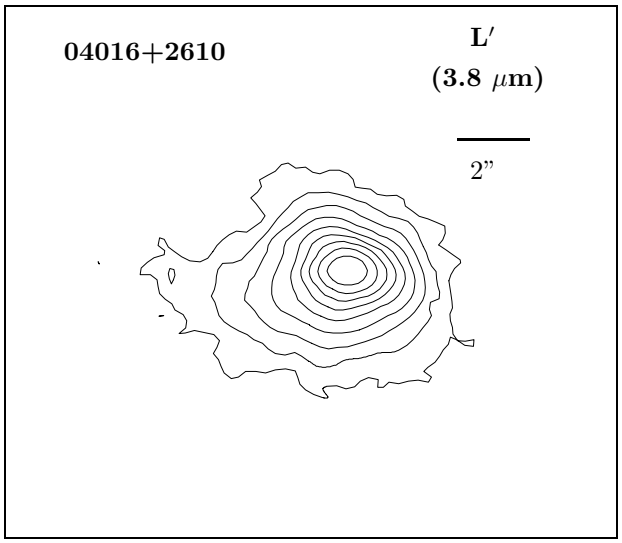

Figure 5

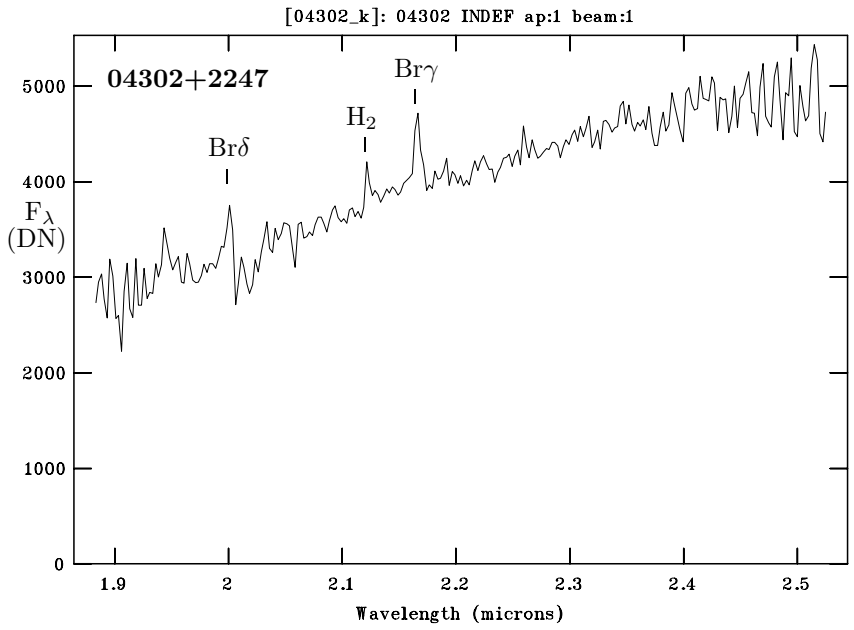
[04302_k]: 04302 INDEF ap:1 beam:1
04302+2247
Brγ
H2
Brδ
Fλ
(DN)
5000
4000
3000
2000
1000
0
1.9
2
2.1
2.2
2.3
2.4
2.5
Wavelength (microns)